CHEMISTRY OF MATERIALS

pubs.acs.org/cm

Article

Reaction Pathway Analysis of B/Li_2O in a Li–B–O System for Boron Nitride Nanotube Growth

Kai Zhang,[▽] Pan Xue,[▽] Jianghua Wu,[▽] Liyun Wu,[▽] Nanyang Wang, Tao Xu, Kaiping Zhu, Jun Pu, Qiulong Li, Yu Deng, Yagang Yao,* and Jin Zhang

Cite This: *Chem. Mater.* 2023, 35, 4857–4864

Read Online

ACCESS | Metrics & More | Article Recommendations | Supporting Information

ABSTRACT: Compared to other synthetic methods, the synthesis of boron nitride nanotubes (BNNTs) by the boron oxide chemical vapor deposition (BOCVD) method can balance the purity and quality of the product nanotubes. However, due to the solid reaction characteristics of boron monomers, the closed reaction system, and the synthesis temperature of over 1000 °C, growth studies of BNNTs have been in a dilemma. To this end, simultaneous thermal analysis combined with multi-atmosphere annealing experiments at corresponding temperatures is used to study the inorganic solid-state reaction of the classical BOCVD precursor B/Li_2O in real time and confirmed by experimental results that lithium borate is the actual active component and catalyst. Further experiments reveal that the growth process of BNNTs and lithium borate not only consumes less of the precursor and ammonia but is also flexible in its configuration, showing exceptional efficiency and reactivity. Lastly, experiments have shown that the structure and activity of borate are equally applicable to alkali metals, alkaline earth metal, and transition metals.

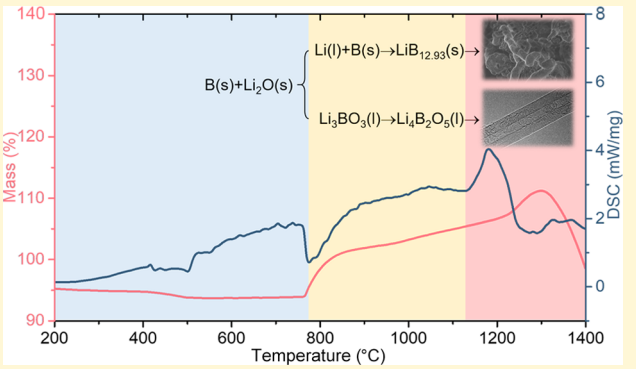

1. INTRODUCTION

Boron nitride nanotubes (BNNTs), the isoelectronic equivalent of carbon nanotubes (CNTs), are first synthesized by arc discharge in 1995,[1] which is only four years after CNTs' first report,[2] but their synthesis and growth mechanisms lagged far behind those of CNTs.[3] The reason for this is that the more reactive gaseous boron sources or boron sources that can be easily vaporized are flammable, explosive, or highly toxic,[4] and although they are more efficient to synthesize, not all research groups can meet the requirements for their use, so more have opted for boron monomer as the boron source.[5−7]

The key to using a solid boron source is to solve the problem of the high melting point of the boron monomer so that it has the opportunity to combine with the nitrogen source. Researchers first think of using techniques such as discharge arcs,[1] high energy lasers,[8] or plasma flames[9] to melt the boron and crack the nitrogen at extremely high temperatures to obtain the boron nitride (BN) structure. Meanwhile, the complexity of these devices makes it easy to add components such as mass spectrometry, optical emission analysis,[10,11] or a high-speed camera[12,13] to allow the in-site analysis of the reactions and substances involved during growth and thus to analyze the growth of BNNTs in conjunction with the composition and structure characterization of the nanoparticles in the tip of the nanotubes. However, while the high reaction temperatures serve to activate the boron, they also exacerbate the intensity of the reaction between the boron and nitrogen sources, resulting in a product that typically contains no more than 50% nanotubes.[10,14]

For the purity of the nanotubes, researchers further developed ball milling and annealing[15] and boron oxide chemical vapor deposition (BOCVD)[16] methods. The ball milling and annealing method increases the activity of the boron through mechanical forces of milling for over 100 h in ammonia and then annealing them under a nitrogen atmosphere to form tubular structures.[17] The BOCVD method is designed as a precursor consisting of boron and metal oxides, which are chemically reacted to form gaseous boron oxides as a boron source for the growth of BNNTs.[18] The high activity of the gas-phase boron source allows for a combination of quality and purity of the product.

However, resolving the growth process of BNNTs has been challenging. In this case, the synthesis with the ball milling and annealing method is divided into two steps, namely, comparative analysis of the structural changes in the composition of the

Received: April 10, 2023
Revised: May 31, 2023
Published: June 12, 2023

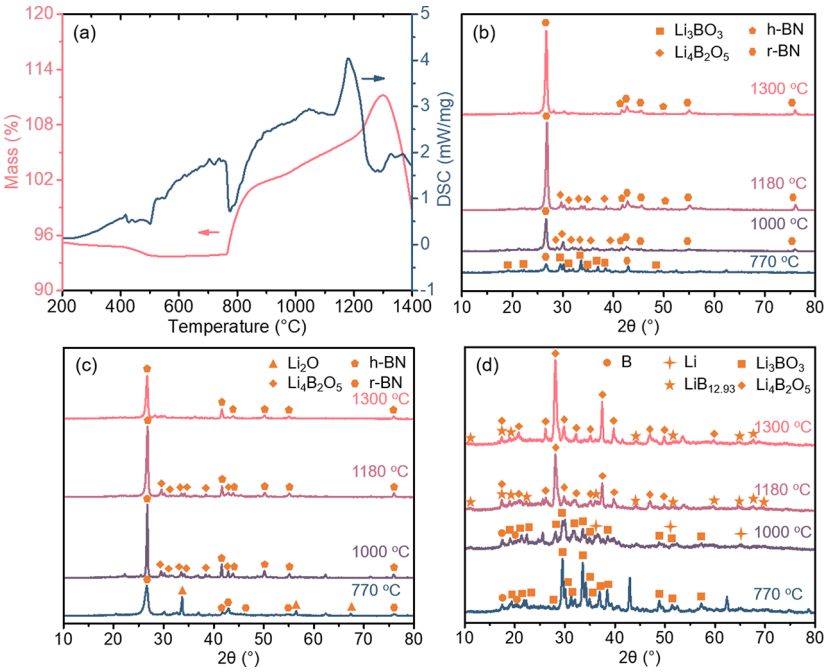

Figure 1. Simultaneous thermal analysis result for B/Li_2O (a) and XRD patterns of B/Li_2O annealing at various temperatures in nitrogen (b), ammonia (c), and argon (d), respectively.

precursors before and after annealing enables gaining some information with the growth process of the BOCVD method taking place entirely inside a confined corundum tube, making it difficult to resolve the reactions within it. To this end, Özmen et al. analyzed the outlet stream using mass spectrometry but found no component directly related to BNNTs.[19] While nanoparticles wrapped in the BNNTs can generally be analyzed as catalysts,[20−22] product analysis also identifies hollow-headed nanotubes,[17,23] making them difficult to recognize as the catalyst for BNNT growth. Additionally, reports are showing that the reaction between boron and metal oxides produces mainly borates, which are inefficient for BNNT growth,[24] while some reports use boron oxide/metal oxides as the precursors and borates as intermediates to obtain BNNTs.[25] Therefore, the academic community is still divided on the growth mechanism of BNNTs in BOCVD, which hinders the synthesis of high-purity and high-quality nanotubes and indirectly leads to a lag in the exploration of the properties and applications.

To this end, we chose the simultaneous thermal analysis technique to simulate the mass change and thermal effects of the reactions of the classical BOCVD precursor B/Li_2O then annealed it under various atmospheres at the corresponding temperatures to obtain the composition of the precursor at each stage of the growth process and combined with literature research and validation experiments to the knowledge that lithium borate is the actual active component and catalyst for the BNNT from B/Li_2O. The growth experiments with various configurations of lithium borate confirmed its considerable reaction efficiency and reactivity. In addition, further experiments also found that borate-catalyzed growth of BNNTs is not only applicable to alkali metals but also borates of alkaline earth and transition metals.

2. EXPERIMENTAL SECTION

2.1. Materials. Amorphous B powder (99%, D50 ≤ 20 μm), $Li_4B_2O_7$ (99.99%), B_2O_3 (98%), and $Zn_3B_2O_6$ were purchased from Shanghai Aladdin Bio-Chem Technology Co., Ltd. Li_2O (99.99%), MgB_2O_4 (98%), and $Na_2B_4O_7$ (99%) were purchased from Shanghai Macklin Biochemical Co., Ltd. NiB_2O_4 (99 + %) was purchased from Heowns Opde Technologies, Ltd., Tianjin. The high-purity gases (Ar, 99.999%; N_2, 99.999%; NH_3, 99.9999%) were purchased from Linde Qiangsheng Gas (Nanjing) Co., Ltd.

2.2. Precursor Preparation. The molar ratio of boron to the metal in the precursor B/Li_2O and B_2O_3/Li_2O used in this study is 3:1, and they are prepared by weighing certain masses of amorphous B powder (or B_2O_3) and Li_2O according to their molar ratio then grinding for at least 15 min in clean agate until they are fully mixed. Other borate precursors are utilized as received without any additional treatment. If not specified, the precursors used are ∼300 mg per growth.

2.3. Precursor Annealing. To analyze the reaction process of the components, the precursors are annealed at different temperatures under Ar, N_2, and NH_3, respectively. For annealing experiments in NH_3, the entire system is purged with Ar for 3 min before heating the system and removing the samples for safety reasons. The annealing experiments at 770 °C are conducted in a conventional tube furnace (OTF-1200X-S, Hefei Kejing Material Technology Co., Ltd.), while the annealing at 1000, 1180, and 1300 °C is finished in a high-temperature tube furnace (SK-G08163-2-600, Tianjin Zhonghuan Furnace Corp.) due to the highest temperature limit of the tube furnaces. This high-temperature tube furnace is also used for the growth of BNNTs with distinct corundum tubes used for the annealing experiments to ensure identical growth conditions.

2.4. BNNT Synthesis. The growth of BNNTs was performed in a dual-zone high-temperature tube furnace with an outer diameter of ∼80 mm. In this case, the first temperature zone along the flow direction is used only for the gas preheating, and a BN ark containing the precursor and substrate is in the middle of the second zone. Before the furnace is heated up, the precursor is spread uniformly over the bottom of the BN ark, which is then covered with a corundum/sapphire substrate and brought to the center of the second temperature zone of the furnace. After that, the flow meter is switched to the cleaning mode and the system is flooded for 3 min to remove the air then the system begins to heat up. The system is heated in a pure Ar atmosphere. When the temperature reached 1300 °C, the gas flow is switched to NH_3 to begin the growth process, the growth duration is 0.5−2 h depending on the experimental requirements. After that, the system is cooled down to room temperature in Ar, and the BNNT-deposited substrates and precursor residues are collected separately for further analysis.

https://doi.org/10.1021/acs.chemmater.3c00838
Chem. Mater. 2023, 35, 4857−4864

2.5. Characterizations. A field emission scanning electron microscope (SEM, Hitachi SU8100) is used for morphology analysis. A transmission electron microscope (TEM, FEI G2 F20 S-TWIN +Aztec X-MAX 80 T) equipped with energy-dispersive X-ray spectroscopy (EDX) and electron energy loss spectroscopy (EELS) is employed to collect the microscopic morphology and element distribution information. Powder X-ray diffraction (XRD, Shimadzu D8 Advance) is utilized for crystallographic analysis. A Raman spectrometer equipped with a 532 nm laser (HORIBA Jobin Yvon, LABRAM HR) is used to collect compositional data. Simultaneous thermal analysis (NETZSCH 449F3) is employed for thermophysical analysis. X-ray photoelectron spectroscopy (XPS, Thermo Scientific K-Alpha) is used to acquire the surface element composition and chemical state analysis.

3. RESULTS AND DISCUSSION

The thermogravimetry (TG) and differential scanning calorimetry (DSC) results of the simultaneous thermal analysis are presented in Figure 1a. It can be seen that the precursor weight sharply increases between 750 and 870 °C, continues to increase until 1200 °C, and then rapidly raises again until 1300 °C. Calculations show that a complete conversion of boron in the precursor to BN results in an 18.87% weight increase, which is marginally higher than the 17.57% increase observed in the TG curve. This suggests that the precursor is highly reactive and may bind to nitrogen with a dissociation energy of up to 945 kJ/mol[4] at only 750 °C. The DSC curve indicates two chemical reactions. The first reaction absorbs 351.9 J/g of heat at 750−760 °C and coincides with a weight increase, while the second reaction releases 694.1 J/g of heat at 1150−1180 °C and causes another weight increase.

To explore specific reactions and confirm BN formation, the precursor was annealed in nitrogen at four temperatures (770 °C for the fastest weight increase, 1180 °C for the most intense exothermicity, 1300 °C for the maximum weight, and 1000 °C as the transition between). XRD analysis shows that B (PDF no. 031-0207; Figure S1) and Li_2O (PDF no. 073-0593; Figure S1) change into r-BN (PDF no. 045-1171) and lithium borate (Figure 1b). The structure of lithium borate evolves with the temperature, which is Li_3BO_3 (PDF no. 018-0718) at 770 °C then transforms to $Li_4B_2O_5$ (PDF no. 018-0719) between 1000 and 1180 °C and disappears altogether by 1300 °C. To replicate the BNNTs' growth environment, the above experiments were repeated in ammonia. The results show that lithium borate's crystal phase is unchanged while that of r-BN becomes h-BN (PDF no. 034-0421) due to ammonia's higher activity (Figure 1c). From this, it can be speculated that lithium borate may serve as an essential mediator between the precursor and nitrogen source, which is consumed at 1300 °C, leaving only BN in the residue.

To further exclude interference from the nitrogen source, the precursor was annealed in argon. The results indicate that lithium borate is its primary constituent with increasing the temperature causing crystal phase transition (Li_3BO_3 from 770 to 1000 °C and $Li_4B_2O_5$ from 1180 to 1300 °C; Figure 1d). Meanwhile, B and Li (PDF no. 089-3940) appear between 770 and 1000 °C whereas $LiB_{12.93}$ (PDF no. 083-0166) at higher temperatures of 1180−1300 °C, offering new insights into precursor evolution.

The above results suggest that B and Li_2O undergo a redox reaction to produce Li_3BO_3 and Li (reaction 1) followed by the conversion of the crystalline form of Li_3BO_3 to $Li_4B_2O_5$ (reaction 2), which releases Li_2O at a higher temperature. Meanwhile, the byproduct of reaction 1, that is, Li, combines with excessive B and forms $LiB_{12.93}$ (reaction 3).[26] Li_3BO_3 and $Li_4B_2O_5$ rapidly react with nitrogen or ammonia to form BN (reactions 4−7), while $LiB_{12.93}$ also binds with them to become BN (reactions 8 and 9). The specific chemical equations for the above reactions are provided in the Supporting Information.

For the reasonableness of these reactions, the enthalpy change of reactions 1 and 2 is calculated by FactSage's web version and confirmed their thermal effects matching the DSC curve. Thermal effects of the side reactions are also considered: Bukovec et al.'s findings showed that the peak position in the DSC curve did not match the reaction temperature of B/Li (reaction 3) due to the fact that it should occur below 700 °C;[27] the TG curve continues to rise after 750 °C, suggesting that reactions 4−9 should not be reflected in the DSC curve. The conversion of Li_3BO_3 to $Li_4B_2O_5$ causes the Li content to rise because of the difference in the volatilization rates between B_2O_3 and Li_2O in lithium borate.[28] This reaction pathway is summarized in Figure 2.

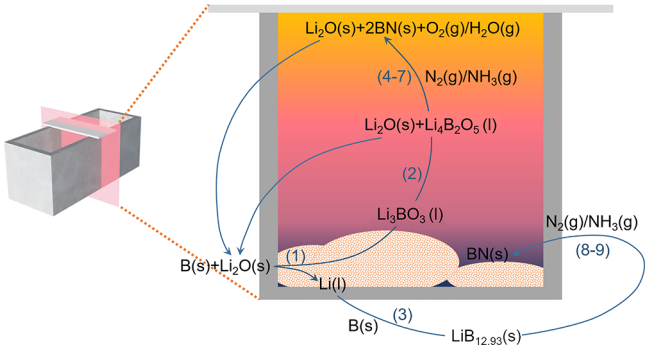

Figure 2. Schematic diagram of the reaction pathway of B/Li_2O.

The above reaction pathway indicates that lithium borate is the actual active component in the Li−B−O system. To confirm this, commercial lithium borate-$Li_2B_4O_7$ was used as the precursor to growing BNNTs and compared with products from argon-annealed B/Li_2O and B/Li_2O. SEM images at low and high magnification show that the collected products are uniformly distributed on the substrate without agglomerates or heterogeneities (Figure 3a−f). All three precursors produce highly pure one-dimensional nanostructures with identical morphologies whose lengths are beyond the view of these SEM images. TEM analysis reveals these structures to be hollow tubes with a wall spacing of ∼0.34 nm, which is consistent with reported BNNTs (Figure 3g−i).[29,30] Raman analysis detected peaks at 1364−1365 cm^{-1} corresponding to the counter phase vibrational mode (E_{2g}) within the BN sheet[31] (Figure 3j−l), confirming that these tubes are BNNTs. In addition, the full width at half-maximum (FWHM) values of the Raman signals of the products are 13.3, 13.7, and 19.1 ($Li_2B_4O_7$ < annealed B/Li_2O < B/Li_2O; Figure 3j−l), the diameters of their nanotubes are 7.1−9.3, 9.3−10, and 9.3−14.1 nm in order, and the wall numbers are 8−11, 10−11, and 11−13 in order, respectively (Figure 3g−i and Figure S2). The BNNTs grown from lithium borate own narrower FWHMs, smaller tube diameters, and fewer wall numbers, suggesting that the product of lithium borate is not only of superior quality and crystallinity compared to B/Li_2O but also the nanotubes obtained have fewer walls and smaller diameters than existing low-temperature schemes.[18,32−35]

https://doi.org/10.1021/acs.chemmater.3c00838
Chem. Mater. 2023, 35, 4857−4864

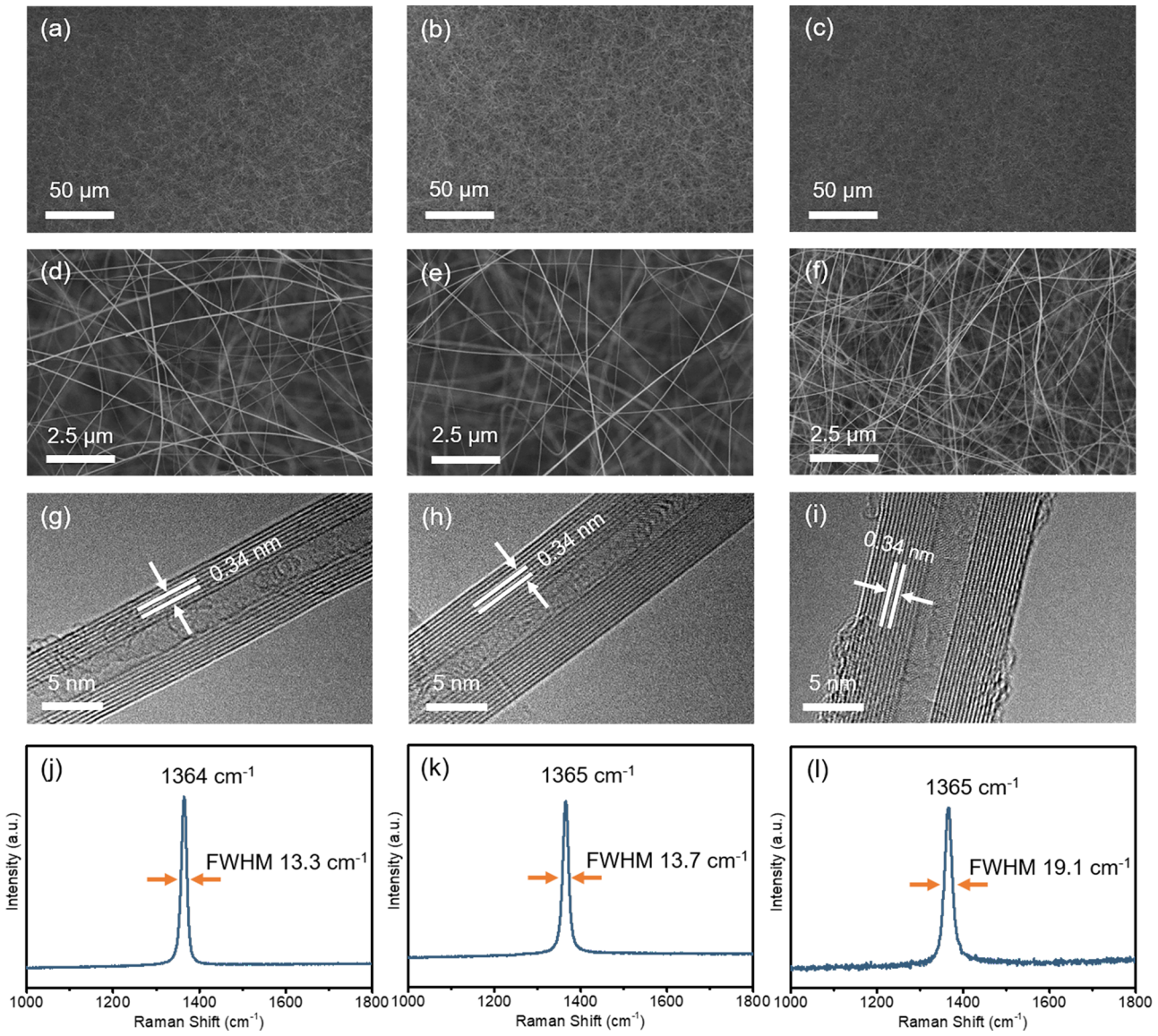

Figure 3. SEM images, TEM images, and Raman spectra of BNNTs grown from $Li_2B_4O_7$ (a, d, g, j), Ar annealed B/Li_2O (b, e, h, k), and B/Li_2O (c, f, i, l).

The residues of $Li_2B_4O_7$ and B/Li_2O were further analyzed to investigate their differences in BNNT growth. Among them, $Li_2B_4O_7$ residue was found to mainly consist of clusters covered by sheets (Figure 4a), while B/Li_2O residue had twisted fibers with varying diameters (Figure 4b). The XRD patterns revealed that both have h-BN as the primary component (Figure 4c,d) and Li_3BO_3 along with $Li_4B_2O_5$ in the case of $Li_2B_4O_7$'s residue (Figure 4c).

For B/Li_2O, reactions 1−3 exist simultaneously. Reactions 1 and 2 produce lithium borate, volatilize into the system, and combine with ammonia to form BNNTs (reactions 6 and 7). Meanwhile, reaction 3 forms $LiB_{12.93}$, which remains solid[26] and does not contribute to BNNT growth. The residue morphology and crystalline phase resemble those of products obtained from B and Li (Figure S3). These fibers likely result from the reaction between $LiB_{12.93}$ and ammonia (reaction 9).

For $Li_2B_4O_7$, it melts completely at 917 °C according to the binary phase diagram of Li_2O-B_2O_3.[36] DSC analysis shows that it begins melting with a weight loss at around 915 °C due to heat absorption,[37] which is consistent with results from argon

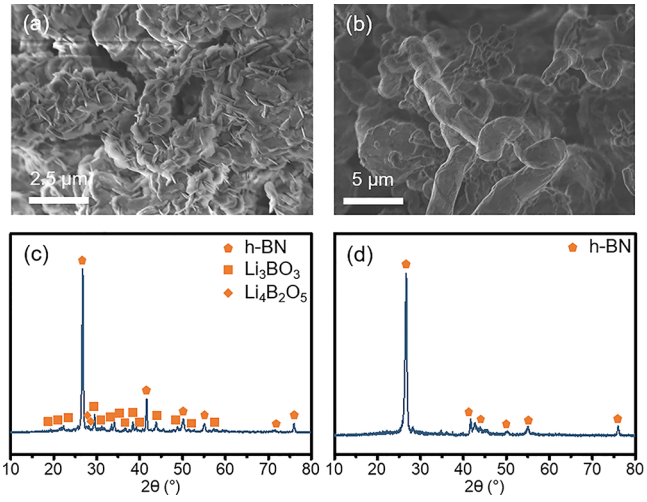

Figure 4. SEM images and XRD patterns of the residue grown with $Li_2B_4O_7$ (a, c) and B/Li_2O (b, d).

https://doi.org/10.1021/acs.chemmater.3c00838
Chem. Mater. 2023, 35, 4857−4864

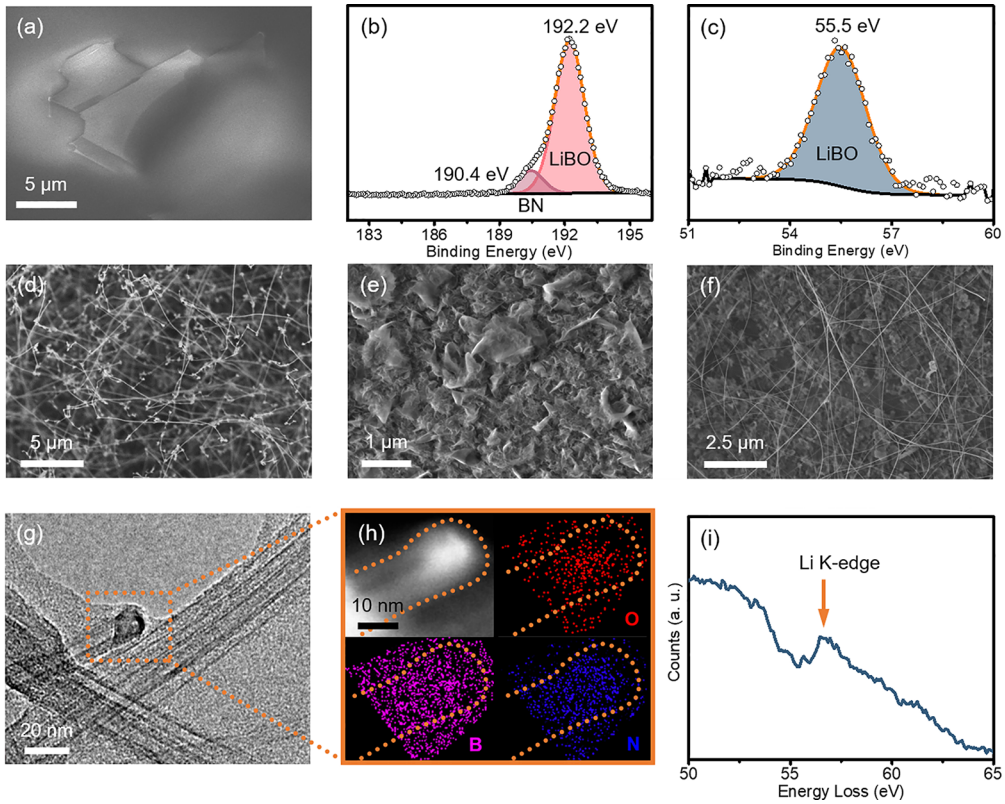

Figure 5. SEM image (a), B 1s (b), and Li 1s (c) XPS fine spectra of the collected deposits on the substrate and SEM image (d) of this substrate after growth in ammonia. SEM image (e) of pure B_2O_3 after growth. SEM image (f) of separated B_2O_3 and Li_2O after growth; the setup is illustrated in Figure S9. TEM image (g) of a BNNT tip and corresponding EDX mapping image (h) and EELS spectrum (i).

annealing experiments (Figure S4). During growth, $Li_2B_4O_7$ remains as a liquid and the volatilized gas components react with ammonia to form BNNTs. Upon cooling, droplets solidify into clusters and react with residual ammonia, forming BN sheets on their surfaces (Figure 4a).

During our study on the thermal properties of lithium borate, we found that it can be expressed as a certain ratio of Li_2O and B_2O_3,[36,37] such as $Li_2B_4O_7$ in $Li_2O{\cdot}2B_2O_3$, $Li_4B_2O_5$ in $2Li_2O{\cdot}B_2O_3$, and Li_3BO_3 in $1.5Li_2O{\cdot}0.5B_2O_3$. Utilizing this information, we formulated a B_2O_3/Li_2O precursor with the same molar ratio as B/Li_2O and found that the results were comparable to the product of $Li_2B_4O_7$ (Figure S5). Using only a 25 mg precursor and feeding 25 sccm of ammonia gas in 30 min of growth can produce BNNTs that cover the substrate toward the precursor (Figure S6). BNNTs can be grown for up to 17 cycles without adding any precursors but ammonia after predeposition (Figures S7 and S8). Compared to existing reports, BNNT synthesis using lithium borate requires less precursor, has a shorter growth time, is sensitive to ammonia, and has long-lasting effects (Table S1), demonstrating the high activity and efficiency of lithium borate.

For the growth of BNNTs, it is assumed above that they are formed by the volatilization of liquid lithium borate in the system as small nano-sized droplets combined with ammonia. To further confirm if the BNNTs are grown from lithium borate, the volatilized components are collected by a substrate above the precursor. The SEM image shows no distinctive products (Figure 5a). B 1s XPS spectra reveal two states of boron with peaks at 192.2 eV for lithium borate and 190.4 eV for BN (Figure 5b). The Li 1s spectra show a peak at 55.5 eV corresponding to lithium borate as in the B 1s spectra at 192.2 eV (Figure 5c),[38,39] indicating lithium borate vaporization to the system. The BN product comes from the BN ark used for annealing as shown in Figure S4. Further, to determine whether the components on the substrate are capable of growing BNNTs, the substrate is put back into the furnace for BNNT growth. The SEM image of this substrate annealed in ammonia finds one-dimensional nanostructures similar to Figure 3d–f (Figure 5d), demonstrating that lithium borate reacts with ammonia to form BNNTs. As a comparison, B_2O_3 only produces BN sheets (Figure 5e). Moreover, BNNTs are grown by separating B_2O_3 and Li_2O as Figure S9 demonstrates the flexibility of the component configuration when grown with lithium borate (Figure 5f). Data on conventional catalyst validation were also collected, which found that O, B, and N elements in the nanoparticle at the BNNT tip and B and O are aggregated in the center (Figure 5g,h). EELS analysis finds Li in the nanoparticles (Figure 5i).[40,41] Thus, the BNNTs are catalyzed by lithium borate in this work.

Furthermore, to investigate the potential of other borates, MgB_2O_4, NaB_4O_7, NiB_2O_4, and $Zn_3B_2O_6$ were tested for BNNT growth. SEM images showed that all four borates produce one-dimensional nanostructures on the substrate. Of these structures, those formed with MgB_2O_4 exhibit a higher density and quantity (Figure S10a), while sheet-like structures predominated in NaB_4O_7 (Figure S10b). BNNTs and twisted fibers of larger diameters are observed in NiB_2O_4 and $Zn_3B_2O_6$ samples (Figure S10c,d). Raman spectra confirmed that the collected materials are BN (Figure S10e–h). This suggests that borates from alkali metals, alkaline earth metal, and transition metals can facilitate BNNT with magnesium and lithium being

https://doi.org/10.1021/acs.chemmater.3c00838
Chem. Mater. 2023, 35, 4857−4864

particularly active among them based on these experimental results.

4. CONCLUSIONS

In conclusion, we chose B/Li_2O as a representative of the BOCVD system and analyze their weight change and thermal effects in the whole growth process by simultaneous thermal analysis. Accordingly, the heat treatments under N_2, NH_3, and Ar were done in conjunction with theoretical analysis to determine their reaction pathway. It was found and verified that the product of the reaction between the two, namely, lithium borate, is the actual active component and catalyst. Follow-up experiments also revealed that, under the same conditions, lithium borate synthesized BNNTs with a diameter of 7.1 nm, a wall number of 8, and an FWHM of 13.3 cm^{-1}, which are much smaller than those of B/Li_2O. Meanwhile, BNNTs grown from lithium borate can cover the substrate surface toward the precursor with a growth time of 30 min, a precursor dosage of 25 mg, and an ammonia flow rate of 25 sccm and can cycle the growth of BNNTs up to 17 times after pre-deposition of the precursor. Additionally, MgB_2O_4, NaB_4O_7, NiB_2O_4, and $Zn_3B_2O_6$ were also verified to be able to be used for the growth of BNNTs, thus showing the universality of borate as an active component.

■ ASSOCIATED CONTENT

Supporting Information

The Supporting Information is available free of charge at https://pubs.acs.org/doi/10.1021/acs.chemmater.3c00838.

Additional chemical equations, SEM images, TEM images, optical images, XRD patterns, Raman spectra, schematic diagrams, and reported precursor dosage and synthesis conditions (PDF)

■ AUTHOR INFORMATION

Corresponding Author

Yagang Yao − *National Laboratory of Solid State Microstructures, College of Engineering and Applied Sciences, Jiangsu Key Laboratory of Artificial Functional Materials and Collaborative Innovation Center of Advanced Microstructures, Nanjing University, Nanjing 210093, China;* orcid.org/0000-0002-4381-2952; Email: ygyao2018@nju.edu.cn

Authors

Kai Zhang − *National Laboratory of Solid State Microstructures, College of Engineering and Applied Sciences, Jiangsu Key Laboratory of Artificial Functional Materials and Collaborative Innovation Center of Advanced Microstructures, Nanjing University, Nanjing 210093, China*

Pan Xue − *National Laboratory of Solid State Microstructures, College of Engineering and Applied Sciences, Jiangsu Key Laboratory of Artificial Functional Materials and Collaborative Innovation Center of Advanced Microstructures, Nanjing University, Nanjing 210093, China; School of Chemistry and Chemical Engineering, Yangzhou University, Yangzhou 225002 Jiangsu, China*

Jianghua Wu − *National Laboratory of Solid State Microstructures, College of Engineering and Applied Sciences, Jiangsu Key Laboratory of Artificial Functional Materials and Collaborative Innovation Center of Advanced Microstructures, Nanjing University, Nanjing 210093, China; i-Lab, CAS Center for Excellence in Nanoscience, Suzhou Institute of Nano-Tech and Nano-Bionics (SINANO), Chinese Academy of Sciences, Suzhou 215123, China*

Liyun Wu − *National Laboratory of Solid State Microstructures, College of Engineering and Applied Sciences, Jiangsu Key Laboratory of Artificial Functional Materials and Collaborative Innovation Center of Advanced Microstructures, Nanjing University, Nanjing 210093, China*

Nanyang Wang − *National Laboratory of Solid State Microstructures, College of Engineering and Applied Sciences, Jiangsu Key Laboratory of Artificial Functional Materials and Collaborative Innovation Center of Advanced Microstructures, Nanjing University, Nanjing 210093, China*

Tao Xu − *National Laboratory of Solid State Microstructures, College of Engineering and Applied Sciences, Jiangsu Key Laboratory of Artificial Functional Materials and Collaborative Innovation Center of Advanced Microstructures, Nanjing University, Nanjing 210093, China*

Kaiping Zhu − *National Laboratory of Solid State Microstructures, College of Engineering and Applied Sciences, Jiangsu Key Laboratory of Artificial Functional Materials and Collaborative Innovation Center of Advanced Microstructures, Nanjing University, Nanjing 210093, China*

Jun Pu − *National Laboratory of Solid State Microstructures, College of Engineering and Applied Sciences, Jiangsu Key Laboratory of Artificial Functional Materials and Collaborative Innovation Center of Advanced Microstructures, Nanjing University, Nanjing 210093, China; Key Laboratory of Functional Molecular Solids, Ministry of Education, Anhui Provincial Engineering Laboratory for New-Energy Vehicle Battery Energy-Storage Materials, College of Chemistry and Materials Science, Anhui Normal University, Wuhu 241002 Anhui, China;* orcid.org/0000-0001-9393-3798

Qiulong Li − *National Laboratory of Solid State Microstructures, College of Engineering and Applied Sciences, Jiangsu Key Laboratory of Artificial Functional Materials and Collaborative Innovation Center of Advanced Microstructures, Nanjing University, Nanjing 210093, China; College of Materials Science and Engineering, Nanjing Tech University, Nanjing 211816, China;* orcid.org/0000-0003-1102-5900

Yu Deng − *National Laboratory of Solid State Microstructures, College of Engineering and Applied Sciences, Jiangsu Key Laboratory of Artificial Functional Materials and Collaborative Innovation Center of Advanced Microstructures, Nanjing University, Nanjing 210093, China*

Jin Zhang − *Center for Nanochemistry, Beijing Science and Engineering Center for Nanocarbons, Beijing National Laboratory for Molecular Sciences, College of Chemistry and Molecular Engineering, Peking University, Beijing 100871, P.R. China;* orcid.org/0000-0003-3731-8859

Complete contact information is available at: https://pubs.acs.org/10.1021/acs.chemmater.3c00838

Author Contributions

[▽]K.Z., P.X., J.W., and L.W. contributed equally. The manuscript was written through contributions of all authors. All authors have given approval to the final version of the manuscript.

Notes

The authors declare no competing financial interest.

Any additional relevant notes should be placed here.

https://doi.org/10.1021/acs.chemmater.3c00838
Chem. Mater. 2023, 35, 4857−4864

■ ACKNOWLEDGMENTS

This work was supported by the National Natural Science Foundation of China (no. 51972162).

■ ABBREVIATIONS

BNNT, boron nitride nanotubes; CNT, carbon nanotube; BN, boron nitride; BOCVD, boron oxide chemical vapor deposition; SEM, scanning electron microscopy; TEM, transmission electron microscopy; EDX, energy-dispersive X-ray spectroscopy; EELS, electron energy loss spectroscopy; XRD, X-ray diffraction; XPS, X-ray photoelectron spectroscopy; TG, thermogravimetry; DSC, differential scanning calorimetry.

■ REFERENCES

(1) Chopra, N. G.; Luyken, R. J.; Cherrey, K.; Crespi, V. H.; Cohen, M. L.; Louie, S. G.; Zettl, A. Boron Nitride Nanotubes. *Science* **1995**, *269*, 966−967.
(2) Iijima, S. Helical Microtubules of Graphitic Carbon. *Nature* **1991**, *354*, 56−58.
(3) Golberg, D.; Bando, Y.; Huang, Y.; Terao, T.; Mitome, M.; Tang, C.; Zhi, C. Boron Nitride Nanotubes and Nanosheets. *ACS Nano* **2010**, *4*, 2979−2993.
(4) Kim, K. S.; Kim, M. J.; Park, C.; Fay, C. C.; Chu, S. H.; Kingston, C. T.; Simard, B. Scalable Manufacturing of Boron Nitride Nanotubes and Their Assemblies: A Review. *Semicond. Sci. Technol.* **2017**, *32*, No. 013003.
(5) Sen, R.; Satishkumar, B. C.; Govindaraj, A.; Harikumar, K. R.; Raina, G.; Zhang, J. P.; Cheetham, A. K.; Rao, C. N. R. B-C-N, C-N and B-N Nanotubes Produced by the Pyrolysis of Precursor Molecules over Co Catalysts. *Chem. Phys. Lett.* **1998**, *287*, 671−676.
(6) Xu, L.; Peng, Y.; Meng, Z.; Yu, W.; Zhang, S.; Liu, X.; Qian, Y. A Co-Pyrolysis Method to Boron Nitride Nanotubes at Relative Low Temperature. *Chem. Mater.* **2003**, *15*, 2675−2680.
(7) Han, W.; Bando, Y.; Kurashima, K.; Sato, T. Synthesis of Boron Nitride Nanotubes from Carbon Nanotubes by a Substitution Reaction. *Appl. Phys. Lett.* **1998**, *73*, 3085−3087.
(8) Golberg, D.; Bando, Y.; Eremets, M.; Takemura, K.; Kurashima, K.; Yusa, H. Nanotubes in Boron Nitride Laser Heated at High Pressure. *Appl. Phys. Lett.* **1996**, *69*, 2045−2047.
(9) Shimizu, Y.; Moriyoshi, Y.; Tanaka, H.; Komatsu, S. Boron Nitride Nanotubes, Webs, and Coexisting Amorphous Phase Formed by the Plasma Jet Method. *Appl. Phys. Lett.* **1999**, *75*, 929.
(10) Kim, K. S.; Kingston, C. T.; Hrdina, A.; Jakubinek, M. B.; Guan, J.; Plunkett, M.; Simard, B. Hydrogen-Catalyzed, Pilot-Scale Production of Small-Diameter Boron Nitride Nanotubes and Their Macroscopic Assemblies. *ACS Nano* **2014**, *8*, 6211−6220.
(11) Guo, L.; Singh, R. N. Selective Growth of Boron Nitride Nanotubes by Plasma-Enhanced Chemical Vapor Deposition at Low Substrate Temperature. *Nanotechnology* **2008**, *19*, No. 065601.
(12) Cho, H.; Kim, J. H.; Hwang, J. H.; Kim, C. S.; Jang, S. G.; Park, C.; Lee, H.; Kim, M. J. Single- and Double-Walled Boron Nitride Nanotubes: Controlled Synthesis and Application for Water Purification. *Sci. Rep.* **2020**, *10*, 1−10.
(13) Yatom, S.; Raitses, Y. Characterization of Plasma and Gas-Phase Chemistry during Boron-Nitride Nanomaterial Synthesis by Laser-Ablation of Boron-Rich Targets. *Phys. Chem. Chem. Phys.* **2020**, *22*, 20837−20850.
(14) Fathalizadeh, A.; Pham, T.; Mickelson, W.; Zettl, A. Scaled Synthesis of Boron Nitride Nanotubes, Nanoribbons, and Nanococoons Using Direct Feedstock Injection into an Extended-Pressure, Inductively-Coupled Thermal Plasma. *Nano Lett.* **2014**, *14*, 4881−4886.
(15) Chen, Y.; Chadderton, L. T.; Gerald, J. F.; Williams, J. S. A Solid-State Process for Formation of Boron Nitride Nanotubes. *Appl. Phys. Lett.* **1999**, *74*, 2960−2962.
(16) Tang, C.; Bando, Y.; Sato, T.; Kurashima, K. A Novel Precursor for Synthesis of Pure Boron Nitride Nanotubes. *Chem. Commun.* **2002**, *2*, 1290−1291.
(17) Li, L.; Li, L. H.; Chen, Y.; Dai, X. J.; Xing, T.; Petravic, M.; Liu, X. Mechanically Activated Catalyst Mixing for High-Yield Boron Nitride Nanotube Growth. *Nanoscale Res. Lett.* **2012**, *7*, 1−8.
(18) Pakdel, A.; Zhi, C.; Bando, Y.; Nakayama, T.; Golberg, D. A Comprehensive Analysis of the CVD Growth of Boron Nitride Nanotubes. *Nanotechnology* **2012**, *23*, No. 215601.
(19) Özmen, D.; Sezgi, N. A.; Balcı, S. Synthesis of Boron Nitride Nanotubes from Ammonia and a Powder Mixture of Boron and Iron Oxide. *Chem. Eng. J.* **2013**, *219*, 28−36.
(20) Zhong, B.; Huang, X.; Wen, G.; Yu, H.; Zhang, X.; Zhang, T.; Bai, H. Large-Scale Fabrication of Boron Nitride Nanotubes via a Facile Chemical Vapor Reaction Route and Their Cathodoluminescence Properties. *Nanoscale Res. Lett.* **2011**, *6*, 1−8.
(21) Guo, H.; Xu, Y.; Chen, H.; Wang, Z.; Mao, X.; Zhou, G.; Zhang, J.; Wang, S. Synthesis of Multiwall Boron Nitride (BN) Nanotubes by a PVD Method Based on Vapor-Liquid-Solid Growth. *Materials (Basel)* **2020**, *13*, 36.
(22) Wang, L.; Li, T.; Ling, L.; Luo, J.; Zhang, K.; Xu, Y.; Lu, H.; Yao, Y. Remote Catalyzation for Growth of Boron Nitride Nanotubes by Low Pressure Chemical Vapor Deposition. *Chem. Phys. Lett.* **2016**, *652*, 27−31.
(23) Zhi, C.; Bando, Y.; Tan, C.; Golberg, D. Effective Precursor for High Yield Synthesis of Pure BN Nanotubes. *Solid State Commun.* **2005**, *135*, 67−70.
(24) E, S.; Wu, L.; Li, C.; Zhu, Z.; Long, X.; Geng, R.; Zhang, J.; Li, Z.; Lu, W.; Yao, Y. Growth of Boron Nitride Nanotubes from Magnesium Diboride Catalysts. *Nanoscale* **2018**, *10*, 13895−13901.
(25) Matveev, A. T.; Firestein, K. L.; Steinman, A. E.; Kovalskii, A. M.; Sukhorukova, I. V.; Lebedev, O. I.; Shtansky, D. V.; Golberg, D. Synthesis of Boron Nitride Nanostructures from Borates of Alkali and Alkaline Earth Metals. *J. Mater. Chem. A* **2015**, *3*, 20749−20757.
(26) Dębski, A.; Braga, M. H.; Gąsior, W. The B-Li System. Calorimetric and Theoretical Studies. *Arch. Metall. Mater.* **2015**, *60*, 2513−2520.
(27) Marčac-Grahek, T.; Bukovec, P.; Bukovec, N. DSC Analysis of the Reaction between Lithium and Boron. *Thermochim. Acta* **1992**, *194*, 385−389.
(28) Loubser, M.; Strydom, C.; Potgieter, H. A Thermogravimetric Analysis Study of Volatilization of Flux Mixtures Used in XRF Sample Preparation. *X-Ray Spectrom.* **2004**, *33*, 212−215.
(29) Chen, W.; Yu, Y.; Gu, Y.; Ji, Y.; He, J.; Li, Z.; Zheng, G.; Wang, J.; Wu, Y.; Long, F. Controllable Synthesis of Boron Nitride Submicron Tubes and Their Excellent Mechanical Property and Thermal Conductivity Applied in the Epoxy Resin Polymer Composites. *Composites, Part A* **2022**, *154*, No. 106783.
(30) Shiratori, T.; Yamane, I.; Nodo, S.; Ota, R.; Yanase, T.; Nagahama, T.; Yamamoto, Y.; Shimada, T. Synthesis of Boron Nitride Nanotubes Using Plasma-Assisted Cvd Catalyzed by Cu Nanoparticles and Oxygen. *Nanomaterials* **2021**, *11*, 651.
(31) Huang, Y.; Lin, J.; Tang, C.; Bando, Y.; Zhi, C.; Zhai, T.; Dierre, B.; Sekiguchi, T.; Golberg, D. Bulk Synthesis, Growth Mechanism and Properties of Highly Pure Ultrafine Boron Nitride Nanotubes with Diameters of Sub-10 Nm. *Nanotechnology* **2011**, *22*, No. 145602.
(32) He, Q.; Ding, L.; Wu, L.; Zhou, Z.; Wang, Y.; Xu, T.; Wang, N.; Zhang, K.; Wang, X.; Ding, F.; Zhang, J.; Yao, Y. Growth of Boron Nitride Nanotube Over Al-Based Active Catalyst and Its Application in Thermal Management. *Small Struct.* **2023**, *4*, 2200282.
(33) Wang, J.; Li, Z.; Gu, Y.; Du, X.; Zhang, Z.; Wang, W.; Fu, Z. Synthesis of Boron Nitride Nanotubes Using Glass Fabrics as Catalyst Growth Framework. *Ceram. Int.* **2015**, *41*, 1891−1896.
(34) Yu, Y.; Chen, H.; Liu, Y.; Craig, V.; Li, L. H.; Chen, Y. Superhydrophobic and Superoleophilic Boron Nitride Nanotube-Coated Stainless Steel Meshes for Oil and Water Separation. *Adv. Mater. Interfaces* **2014**, *1*, No. 1300002.
(35) Wang, H.; Wang, W.; Wang, H.; Zhang, F.; Li, Y.; Fu, Z. Synthesis of Boron Nitride Nanotubes by Combining Citrate-Nitrate Combus-

https://doi.org/10.1021/acs.chemmater.3c00838
Chem. Mater. 2023, 35, 4857−4864

tion Reaction and Catalytic Chemical Vapor Deposition. *Ceram. Int.* **2018**, *44*, 13959−13966.
(36) Sastry, B. S. R.; Hummel, F. A. Studies in Lithium Oxide Systems: I, Li2O B2O3−B2O3. *J. Am. Ceram. Soc.* **1958**, *41*, 7−17.
(37) Mathews, M. D.; Tyagi, A. K.; Moorthy, P. N. High-Temperature Behaviour of Lithium Borates:: Part I: Characterization and Thermal Stability. *Thermochim. Acta* **1998**, *320*, 89−95.
(38) Hensley, D. A.; Garofalini, S. H. XPS Investigation of Lithium Borate Glass and the Li/LiBO2 Interface. *Appl. Surf. Sci.* **1994**, *81*, 331−339.
(39) Choi, S. H.; Lee, S. J.; Kim, H. J.; Park, S. B.; Choi, J. W. Li2O-B2O3-GeO2 Glass as a High Performance Anode Material for Rechargeable Lithium-Ion Batteries. *J. Mater. Chem. A* **2018**, *6*, 6860−6866.
(40) Liu, D. R. Electron Energy Loss Spectroscopy of LiH with a Scanning Transmission Electron Microscope. *Solid State Commun.* **1987**, *63*, 489−493.
(41) Senga, R.; Suenaga, K. Single-Atom Electron Energy Loss Spectroscopy of Light Elements. *Nat. Commun.* **2015**, *6*, 7943.

https://doi.org/10.1021/acs.chemmater.3c00838
Chem. Mater. 2023, 35, 4857−4864